Published in final edited form as:

Sci Signal. 2023 February 14; 16(772): eadd7220. doi:10.1126/scisignal.add7220.

Palmitoylation of the Parkinson's disease-associated protein synaptotagmin-11 links its turnover to α-synuclein homeostasis†

Gary P. H. Ho[1,*], **Erin C. Wilkie**[1], **Andrew J. White**[1], **Dennis J. Selkoe**[1,*]

[1]Ann Romney Center for Neurologic Diseases, Department of Neurology, Brigham and Women's Hospital and Harvard Medical School, Boston, MA 02115 USA

Abstract

Synaptotagmin-11 (Syt11) is a vesicle trafficking protein that is linked genetically to Parkinson's disease (PD). Likewise, the protein α-synuclein regulates vesicle trafficking, and its abnormal aggregation in neurons is the defining cytopathology of PD. Because of their functional similarities in the same disease context, we investigated whether the two proteins were connected. We found that Syt11 was palmitoylated in mouse and human brain tissue and in cultured cortical neurons, and that this modification to Syt11 disrupted α-synuclein homeostasis in neurons. Palmitoylation of two cysteines adjacent to the transmembrane domain, Cys^{39} and Cys^{40}, localized Syt11 to digitonin-insoluble portions of intracellular membranes and protected it from degradation by the endolysosomal system. In neurons, palmitoylation of Syt11 increased its abundance and enhanced the binding of α-synuclein to intracellular membranes. As a result, the abundance of physiologic tetrameric form of α-synuclein was decreased and that of its aggregation-prone monomeric form was increased. These effects were replicated by overexpression of wild-type Syt11 but not a palmitoylation-deficient mutant. These findings suggest that palmitoylation-mediated increases in Syt11 amounts may promote pathological α-synuclein aggregation in PD.

Introduction

Genome-wide association studies have linked the synaptotagmin-11 (*SYT11*) locus to Parkinson's disease (PD) risk (1–3). Targeted sequencing of the *SYT11* gene has validated this association (4). Syt11 is one of 17 members of the synaptotagmin family of transmembrane vesicle-associated proteins. Structurally, synaptotagmins consist of a short luminal domain, a transmembrane domain, and two cytoplasmic C2 calcium-binding domains (5). However, the Syt11 C2 domains are unable to bind calcium due to their increased flexibility and altered orientations of specific residues (6). Whereas the functions of individual synaptotagmins vary, altogether this class of proteins is broadly involved

*Corresponding author. dselkoe@bwh.harvard.edu (D.J.S.), gho@bwh.harvard.edu (G.P.H.).

Author Contributions: G.P.H. and D.J.S. designed research and analyzed data. G.P.H., E.C.W., and A.J.W. performed research. G.P.H. and D.J.S. wrote and edited the paper.

Competing interests: DJS is a director and consultant to Prothena Biosciences. The other authors declare that they have no conflicts of interest.

in regulating vesicle dynamics, including trafficking and endo- and exocytosis at various intracellular locales (5).

Like most other synaptotagmins, Syt11 is expressed almost exclusively in brain tissue (7). Syt11 resides on vesicles distributed throughout the neuronal cell body, axons, and dendrites, and mediates both anterograde and retrograde vesicular trafficking (8). Functionally, forebrain-specific *SYT11*-knockout mice show impaired synaptic plasticity and memory (conventional, whole-body knockouts are lethal within 24 hours of birth) (8). Others have found that Syt11 inhibits clathrin-mediated and bulk endocytosis (9) and suppresses spontaneous neurotransmission (10). In disease models, over-expression of Syt11 in the substantia nigra of mice results in defective release of dopamine and death of dopaminergic neurons, consistent with its possible role in PD (11).

The functions of Syt11 in vesicle trafficking and recycling are shared by a key player in PD, the neuronal protein α-synuclein (αS). αS is the principal component of Lewy bodies and Lewy neurites, the defining pathology of PD (12). Physiologically, αS binds dynamically to highly curved membranes, such as those in vesicles, by means of its amphipathic helix. In disease, certain pathologic forms of αS bind excessively, distorting vesicle shape and impairing their trafficking (13–16). Accordingly, Lewy bodies contain abundant misshapen membranous structures in addition to the classically described fibrillar proteinaceous aggregates of αS (17).

Given these commonalities between αS and Syt11 in the context of PD, we considered whether a functional link exists between them. We were particularly interested in the possible role of palmitoylation in mediating such a connection. Palmitoylation is the post-translational addition of a long-chain fatty acid, usually palmitate, to cysteines. This modification is known to regulate two other synaptotagmins, Syt1 and Syt7, by targeting the former to the synapse (18) and the latter to the lysosome (19). We have previously shown that although αS itself is not palmitoylated (as it lacks cysteines), inhibition of the depalmitoylase acyl-protein-thioesterase-1 (APT1) substantially mitigates αS pathologic inclusions and neurotoxicity (20), consistent with a role for palmitoylation in the regulation of αS homeostasis. Thus, here we explored whether Syt11 was palmitoylated and what connections the modification might have to αS in PD cytopathology.

Results

Syt11 is palmitoylated at Cys^{39} and Cys^{40}

To determine whether Syt11 is palmitoylated in the brain, we used the acyl-biotin exchange (ABE) method for the isolation of palmitoylated proteins (21, 22). This technique uses hydroxylamine to selectively reverse thioester-linked palmitoyl moieties, enabling their replacement by a thiol-reactive pyridyldithiol-biotin (HPDP-biotin) that may then be used for affinity purification by neutravidin agarose. In brain homogenates from wild-type mice, a robust signal for Syt11 was detected in the ABE assay that was dependent on the presence of hydroxylamine, confirming specificity of the finding (Fig. 1A). PSD-95, a well-studied palmitoylated neuronal protein (23), produced a similar pattern, whereas actin, which is not palmitoylated, did not produce any signal. Using the same method, we showed robust Syt11

palmitoylation in rat primary cortical neurons in culture (Fig. 1B) and human cortical brain tissue (Fig. 1C).

We sought to identify the palmitoylation sites of Syt11. Two other synaptotagmins, Syt1 and Syt7, are known to be palmitoylated (18, 24). In both, the palmitoylated sites are conserved cysteines near the transmembrane domain. Consistent with this, the palmitoylation site predictor algorithm CSS-Palm suggests that Cys^{39} and Cys^{40} in Syt11, adjacent to its transmembrane domain, may be palmitoylated. In contrast, a study demonstrating a site-specific ABE method in the mouse forebrain palmitoyl-proteome identified Cys^{117} in the cytosolic domain of Syt11 (corresponding to human C118S) as the palmitoylated site (25). To differentiate between these possibilities, we transfected human embryonic kidney (HEK) cells with FLAG-tagged human wild-type Syt11 (Syt11-wt-FLAG) or cysteine-to-serine mutants corresponding to the above candidate sites, including a C39S/C40S double mutant. Whereas robust palmitoylation was detected for wild-type Syt11, mutating Cys^{39} and Cys^{40} to serines abolished the ABE signal (Fig. 2, A and B). Mutating Cys^{39} or Cys^{40} individually resulted in reduction, but not complete loss, of the palmitoylation signal, consistent with the interpretation that Syt11 is palmitoylated at both cysteines (Fig. 2, A and B). In contrast, C118S did not alter the degree of palmitoylation, indicating that this was not a modified site (Fig. 2, A and B). Palmitoylation of endogenous SNAP-25 remained unchanged across the transfected conditions (Fig. 2A), demonstrating consistency of the ABE method.

To confirm the physiologic relevance of Cys^{39} and Cys^{40} in neurons, we transduced rat cortical neurons with lentivirus encoding either Syt11-wt-FLAG or the corresponding C39S+C40S double mutant (subsequently referred to as “CS”). ABE analysis demonstrated that, consistent with the HEK cell experiments, Syt11-CS-FLAG in neurons resulted in loss of palmitoylation (Fig. 2C). This was apparent despite the decreased total Syt11-CS-FLAG, as demonstrated by comparing the Syt11-CS-FLAG input signal in the long exposure with that of Syt11-wt-FLAG in the short exposure. A robust palmitoylation (ABE) signal was seen for Syt11-wt-FLAG in the short exposure, yet no signal was apparent for Syt11-CS-FLAG even in the long exposure, despite comparable inputs (Fig. 2C). Together, these results demonstrate physiologic palmitoylation of Syt11 at Cys^{39} and Cys^{40} across multiple neural systems.

Palmitoylation at Cys^{39} and Cys^{40} is required for Syt11 protein stability

The striking and consistent change in Syt11-CS-FLAG levels compared to those of Syt11-wt-FLAG (Fig. 2C) prompted us to further characterize this finding. First, we quantified the degree of decrease in Syt11-CS-FLAG protein abundance by Western blot (WB). We found that Syt11-CS-FLAG levels were approximately 20% those of Syt11-wt-FLAG in both rat neurons (Fig. 3A) and induced pluripotent stem cell (iPSC)-derived, neurogenin-induced human neurons (iNs) from an αS gene (*SNCA*) triplication patient (26) (Fig. 3B). We then asked whether this change was due to decreased protein synthesis or increased degradation. Our experiments so far have employed a lentiviral construct containing the Syt11-FLAG open reading frame followed by an internal ribosomal entry site (IRES) and a ZsGreen marker. We reasoned that defects in transcribing or translating the Syt11-CS-FLAG mRNA should also affect the ZsGreen marker. However, the intensity of ZsGreen fluorescence

was unchanged between Syt11-wt-FLAG and Syt11-CS-FLAG transduced neurons (Fig. 3, C and D), arguing against protein production as the responsible factor. Whereas protein translation downstream of an IRES does not always correlate exactly with that of the upstream gene of interest, in most instances translation becomes less efficient following the IRES. In our case, despite lower Syt11-CS-FLAG levels, ZsGreen was not significantly different, suggesting that less efficient translation was not a contributory factor in our experiments.

Although these data point towards increased degradation as the cause of the lower levels of palmitoylation-deficient Syt11, they do not demonstrate it definitively. To answer this question directly, we performed cycloheximide chase experiments to measure the half-life of wild-type and CS-mutant Syt11. In rat neurons, the half-life of transduced Syt11-wt-FLAG in the presence of cycloheximide was approximately 16 hours (Fig. 3E). However, abrogation of its palmitoylation (by expression of the CS mutant) resulted in marked reduction of Syt11's half-life such that by 4 hours, more than 80% of the protein had been degraded (Fig. 3E). The half-life of endogenous GAPDH was unchanged in neurons transduced with either Syt11-wt-FLAG or Syt11-CS-FLAG (Fig. 3F), indicating that this was not due to non-specific effects on the protein degradation machinery.

Protein turnover may be regulated principally by either the ubiquitin-proteasome or endolysosomal systems, with cytosolic proteins generally degraded by the former and membrane-bound proteins by the latter (27). We explored which of these may be responsible for Syt11 degradation. Inhibition of the proteasome with either epoxomicin or MG132 did not affect the levels of Syt11-CS-FLAG (Fig. 3G). In contrast, inhibition of lysosomal function with bafilomycin A increased the amount of Syt11-CS-FLAG protein (Fig. 3G), indicating that the endolysosomal system is primarily responsible for Syt11 turnover. Accumulation of the lipidated form of the autophagasome marker LC3 (LC3-II) in the bafilomycin A-treated cells (Fig. 3G) demonstrated effective inhibition of the lysosome. Together, this series of experiments shows that palmitoylation of Syt11 is required for maintenance of its normal half-life, as regulated by the endolysosomal system.

Syt11 palmitoylation targets Syt11 to digitonin-insoluble portions of membranes

The increased susceptibility of palmitoylation-deficient Syt11 to endolysosomal-mediated degradation led us to consider whether palmitoylation might alter the subcellular distribution of Syt11. First, we confirmed that lentivirally transduced Syt11-wt-FLAG, like endogenous Syt11, formed punctate structures throughout the neuronal soma, axons, and dendrites (Fig. 4A) as previously reported (8). We then compared the distribution of Syt11-wt-FLAG to that of Syt11-CS-FLAG (Fig 4B). Despite attempting to compensate for the lower levels of Syt11-CS-FLAG by transducing lentivirus at a higher multiplicity of infection (20 vs 5 for wt), overall expression of Syt11-CS-FLAG was still substantially reduced. Despite this, both Syt11-wt-FLAG and Syt11-CS-FLAG were found in broadly distributed punctate structures, which were less obvious in the case of Syt11-CS-FLAG due to lower amounts of protein but nevertheless present (Fig. 4B). This point is made clearer by comparing an artificially brightened image of Syt11-CS-FLAG to the untouched Syt11-wt-FLAG (Fig. 4B).

Because abrogating palmitoylation did not broadly affect Syt11 subcellular localization, we explored whether palmitoyation instead targets Syt11 to distinct membrane subdomains. These subdomains may be too close physically to be distinguished by microscopy but may be differentiated based on their biochemical characteristics. To address this question, we performed in situ digitonin extraction experiments (28) in HEK 293T cells expressing either Syt11-wt-FLAG, Syt11-CS-FLAG, or Syt11-C118S-FLAG. Because Syt11 has a transmembrane domain and is, by definition, membrane anchored, we used extractability by digitonin not as a means of distinguishing between cytosolic and membrane localization but as a method to empirically separate digitonin-soluble and -insoluble membrane subdomains. These subdomains insoluble in non-ionic detergents (such as digitonin) are cholesterol-rich, ordered areas of the membrane to which palmitoylated proteins are often targeted and from where they mediate trafficking and receptor signaling functions (29). Whereas Syt11-wt-FLAG was largely digitonin insoluble, a substantial portion of the Syt11-CS-FLAG could be extracted by digitonin (Fig. 4C). In contrast, the C118S mutant, which did not affect palmitoylation, had similar properties as wild-type Syt11 (Fig. 4C). We confirmed these findings in human iNs. As in the 293T cells, wild-type Syt11 showed increased resistance to digitonin extraction compared to the palmitoylation-deficient mutant (Fig. 4D), despite lower overall levels. Thus, palmitoylation targets Syt11 to digitonin-insoluble portions of membranes.

Palmitoylated Syt11 impairs αS homeostasis

In addition to modulating properties of the modified proteins themselves, palmitoylation can also affect the local interacting membrane environment. In particular, the fatty acid chains of palmitoylated proteins can induce curvature of the lipid bilayer, likely through a biophysical interaction of the fatty acid chains with the phospholipids (30, 31). αS binds to certain highly curved membranes through its amphipathic helix and can thereby affect vesicle trafficking (13, 15, 32, 33). Because Syt11 is also localized to intracellular vesicles (8), we investigated whether the presence or absence of palmitoylated Syt11 could affect the dynamic binding of αS to these curved membranes. To address this disease-relevant question, we turned once again to human iPSC-derived iNs from patients with familial PD that harbor a triplication in the gene encoding αS (*SNCA*) (26). Expression of palmitoylation-competent Syt11 (wt), but not palmitoylation-deficient Syt11 (CS mutant), resulted in higher membrane association of αS (decreased cytosol to membrane ratio; Fig. 5A). This was also the case in the corrected version of these patient-derived neurons (Fig. 5B), in which the start codons for two *SNCA* alleles are disrupted by CRISPR/Cas (26, 34).

Changes in the membrane association of αS have been associated with disruptions in the normal ratio of physiologic α-helical αS tetramers to aggregation-prone monomers (35, 36). Thus, we asked whether the palmitoylation state of Syt11 can also affect the equilibrium between the αS tetramer (of 60 kDa; hereafter, αS60) and its monomer (of 14 kDa; hereafter, αS14). Using a well-established in vivo cross-linking method (37–39), we observed that in αS triplication patient-derived neurons, expression of Syt11-wt-FLAG, but not palmitoylation-deficient Syt11-CS-FLAG, decreased the tetramer to monomer (αS60:40) ratio by approximately 30% (Fig. 5C). In contrast, the relative dimerization of endogenous DJ-1, a control protein not known to be affected by Syt11 or αS, was

unchanged in the same cells, arguing against a non-specific effect of Syt11 (Fig. 5C). The αS60:40 ratio was similarly reduced by Syt11-wt-FLAG but not Syt11-CS-FLAG in the genetically corrected version of these neurons (Fig. 5D). Given these effects of Syt11 on αS state, we then considered whether Syt11 binds directly to αS. However, in rat neurons transduced with Syt11-wt-FLAG, we did not detect any specific interaction with αS (fig. S1). Thus, Syt11 alters the membrane binding properties and homeostasis of αS in a palmitoylation-dependent manner without direct binding to αS, possibly through changes in local membrane environment.

Syt11 effect on αS homeostasis can be dissociated from αS phosphorylation

αS tetramers and related multimers in neurons have consistently been found to be physiologic, distinct from any pathologic oligomers of the aggregation-prone monomer (37, 39–41). In contrast, phosphorylation of αS at Ser^{129} ($pSer^{129}$ αS) is an important but unsettled aspect of αS biology, with some studies suggesting a role for it in normal physiology (42–44) and others implicating a role for it in PD pathogenesis (45, 46). Having shown an effect of Syt11 expression on the αS tetramer:monomer balance (Fig. 5), we investigated whether $pSer^{129}$ αS was also affected. In αS-triplication iNs, in corrected iNs, and in rat neurons, we did not see any effect of Syt11-wt-FLAG or Syt11-CS-FLAG expression by lentiviral transduction on $pSer^{129}$ αS levels (Fig. 6, A to C). However, neurogenerative diseases like PD can develop from subtle contributing factors that act over decades of life that may not be apparent from the mere weeks-long time scale of cells in culture. Without a longer-term model, we instead wondered whether detectable changes in $pSer^{129}$ *could* be elicited with greater over-expression of Syt11 over an even shorter period. For this, we turned to transient transfection in HEK cells, in which transiently transfected Syt11 reaches levels approximately 10- to 20-fold higher than that in the iNs (Fig. 6D). In HEK cells expressing high levels of αS-wt by transient transfection, the co-transfection of Syt11-wt-FLAG substantially increased the abundance of $pSer^{129}$ αS, whereas expression of Syt11-CS-FLAG did not achieve the same effect (Fig. 6E). Expression of C118S-mutant Syt11, which does not affect its palmitoylation, increased the abundance of $pSer^{129}$ αS in a manner that was indistinguishable from that by expression of wild-type Syt11 (Fig. 6E). Phosphorylation of the familial PD αS mutant αS-E46K (47), which exhibits higher levels of $pSer^{129}$ αS compared to αS-wt (48), was influenced by Syt11 in a similar way as αS-wt, with Syt11-wt-FLAG, but not palmitoylation-deficient Syt11 or the C118S-mutant, increasing $pSer^{129}$ of αS-E46K (Fig. 6E). Expression of Syt1 or the structurally closely related Syt4 (6) did not alter $pSer^{129}$ levels, unlike Syt11 wt (Fig. 6F), suggesting that this effect was specific to wt Syt11. Given that there was no effect on $pSer^{129}$ αS levels in the same cells in which (palmitoylatable) Syt11 affected the tetramer:monomer equilibrium of αS, the findings indicate that αS assembly state and its phosphorylation status may be dissociated in the context of Syt11. However, it remains to be determined whether these states are as well dissociated in the decades-long context of human PD.

Discussion

The disruption of vesicle trafficking is a fundamental feature of PD biology (14). αS binds to vesicle membranes and accounts for many of these effects in the disease (14, 15, 49).

Recent work on Syt11 has demonstrated that it is also involved in vesicle trafficking (8). Our study demonstrates a link between Syt11 and αS, mediated by palmitoylation of Syt11. Combined with our previous work connecting palmitoylation with cellular pathologies caused by αS, our new findings add further evidence to the overall hypothesis that palmitoylation is a regulator of multiple pathways involved in vesicle dynamics relevant to PD.

Our data provide evidence that Syt11 undergoes palmitoylation and pinpoint where in the protein this occurs. One striking result from our experiments is the rapid degradation of the Syt11-CS palmitoylation deficient mutant. Although palmitoylation is better known for targeting proteins to the membrane or membrane subdomains, there is some precedent for palmitoylation also being required for protein stability (29). However, in the case of the other two known palmitoylated synaptotagmins, Syt1 and Syt7, palmitoylation targets them to specific subcellular compartments and does not play a role in protein turnover (18, 19). This difference is consistent with the growing recognition that despite structural similarities, the synaptotagmins have highly specialized and distinct functions subject to different modes of regulation (5).

We found that the palmitoylation-deficient mutant of Syt11 is degraded rapidly through the endolysosomal system, without any changes in protein levels following proteasomal inhibition. Our result contrasts with a prior work which reported that Syt11 is ubiquitinated by parkin and degraded by the proteasome (50). This may be explained by the use of over-expressed parkin in HEK cells in the prior work, which may allow for parkin-dependent ubiquitination of non-physiologic substrates (51). Mechanisms of protein turnover may also be different in HEK cells compared to neurons. Indeed, we found that Syt11-CS-FLAG levels were unaffected in HEK cells (Fig. 6E), in contrast to what we saw in rat and human neurons (Fig. 3, A and B). Further, the notion that Syt11 may not be a normal substrate of parkin is supported by the absence of Syt11 in several subsequent unbiased proteomic datasets of parkin substrates in neurons (52–54).

We demonstrate here that Syt11 affects αS homeostasis in a manner that requires intact palmitoylation sites (Cys^{39} and Cys^{40}). These sites are shown to be required for both Syt11 protein stability and its localization to digitonin-resistant areas of the membrane. Because mutation of Cys^{39} and Cys^{40} cannot differentiate between these two functions, our data did not specifically attribute the effect of Syt11 on αS to one or the other. In future experiments, it may be possible to identify an alternate mutant that can dissociate the two functions to define more precisely which is most relevant to αS. For example, a constitutively prenylated mutant of Syt11 containing C39S+C40S may still localize to the digitonin-resistant areas of the membrane but could still be subject to more rapid endolysosomal degradation due to its lack of palmitoylation. Although this might be of mechanistic interest, from a functional perspective it does not substantially change the broader finding that palmitoylation of Syt11 affects αS homeostasis, with its associated disease implications.

As part of our analysis, we examined both αS tetramers and αS phosphorylation at Ser^{129}. Decreased abundance of αS tetramers (αS60), resulting in an increase in aggregation-prone monomers (αS14), is consistently associated with human synucleinopathies like PD, DLB

and Gaucher's-PD (37, 39–41). In contrast, the role of pSer^{129} αS is less clear, despite the abundance of this species in Lewy bodies (55). Thus, although an abnormally decreased αS60:40 ratio is often associated with increased pSer^{129} (56–58), this is not always the case. The more recently described familial PD αS-G51D mutant is one such example, in which a decreased αS60:14 ratio is not associated with increased pSer^{129} αS (36). Our results show that in addition to mutants of αS itself, proteins which regulate its function like Syt11 can selectively alter αS homeostasis without increasing pSer^{129} αS.

In our prior work we had demonstrated that inhibition of the depalmitoylase APT1 increases palmitoylation of MAP6, a microtubule binding protein which also traffics with vesicles, and this reduces αS phosphorylation, inclusions, and cytotoxicity (20). This would imply a salutary effect of MAP6 palmitoylation. In contrast, palmitoylated Syt11 decreases physiologic αS tetramers and is therefore predicted to be associated with disease. These results suggest, unsurprisingly, that the fundamental process of palmitoylation has diverse effects depending on the specific proteins and pathways involved. Considering our results with Syt11 and MAP6, it is likely that palmitoylation intersects in additional complex ways with αS in PD biology. From a therapeutic development perspective, targeting the palmitoylation cycle of Syt11 may be of benefit in PD. In particular, inhibition or genetic knockdown of the specific zDHHC palmitoyltransferase responsible for Syt11 may reduce its palmitoylation levels and restore αS homeostasis. Such an approach is underway in our laboratory.

The variants in Syt11 associated with PD are in non-coding regions of the gene (4). It is unclear whether these would lead to increased or decreased expression of Syt11. Based on our findings, we speculate that even slightly increased levels of Syt11, over the many years required for development of neurodegenerative disease, would eventually lead to αS dyshomeostasis and PD. This would be consistent with previous reports showing that over-expression of Syt11 inhibits vesicle pool recycling, inhibits dopamine release, and causes neurotoxicity in mouse substantia nigra (11). To test the disease relevance of these data, future work examining levels of Syt11 in autopsy brain samples from PD patients would be informative.

Together, our experiments demonstrate that palmitoylation of Syt11 is an important biological event that regulates both Syt11 protein turnover and αS homeostasis in the context of PD. This work begins to bring mechanistic clarity to the role of Syt11 in disease and provides further evidence that palmitoylation influences multiple pathways in the biology of αS.

Materials and Methods

Antibodies.

Antibodies used included rodent Syt11 (rabbit, Synaptic Systems 270 003), human Syt11 (mouse, Sigma WH0023208M3, 4E1), PSD-95 (mouse, MilliporeSigma, CP35 7E3-1B8), SNAP-25 (rabbit, Abcam AB5666), human αS (mouse, Thermo Fisher 4B12), human pSer^{129} αS (rabbit, Abcam MJF-R13), rodent/human αS (mouse, Syn1, BD 610787), actin (rabbit, Sigma AC-15), FLAG (mouse, Sigma M2), GAPDH (rabbit, Abcam 181602,

EPR16891), LC3B (rabbit, ThermoFisher, NB1002220), calnexin (rabbit, Sigma C4731), Na/K ATPase (mouse, Abcam 7671), DJ-1 (rabbit, (37)).

cDNA Constructs and lentiviruses.

For transient transfection, plasmids for pCMV6-Syt11-FLAG (RC205445), Syt1 (RC208938), Syt 4 (RC206304), and their corresponding empty vector pCMV6-entry (PS100001) were purchased from Origene. The C39S, C40S, C39S+C40S, and C118S mutants were custom made by Origene in the pCMV6-entry vector. For lentivirus, the Syt11-wt-3xFLAG and Syt11-CS-3xFLAG ORFs were synthesized (Azenta) and cloned into the SpeI-NotI sites in the pLVX-EF1α-IRES-ZsGreen lentiviral vector (Takara #631982) followed by generation of lentiviral particles by Alstem (Richmond, CA). Lentiviral particles were introduced to rat neurons between days 5 to 7 in vitro (DIV5-7) and to iNs between DIV6-8.

Cell Culture.

HEK cells were cultured at 37°C in a 5% CO_2 atmosphere in Dulbecco's modified Eagle's medium (DMEM) supplemented with 10% FBS, 100 units/mL penicillin, 100 μg/mL streptomycin, and 2 mM GlutaMAX supplement (Gibco).

Preparation of primary rat cortical neurons.

Primary neurons were cultured from E18 Sprague-Dawley rats (Charles River Laboratories). All animal care was in accordance with institutional guidelines. Rats were euthanized with CO_2 followed by thoracotomy. Embryonic cortices were isolated and dissociated with trypsin/EDTA and trituration. Cells were plated in Neurobasal medium supplemented with B-27, 2 mM GlutaMAX, 10 units/mL of penicillin, and 10 μg/mL of streptomycin on poly D-lysine coated plates. Subsequently, half the medium was removed and replaced with fresh Neurobasal medium as above but without antibiotics twice weekly for maintenance of cultures. Rat neurons were used for experiments between DIV16-19.

Induced neurons (iNs).

The *SNCA* triplication iPSC line was obtained from The European Bank for induced pluripotent Stem Cells (EBiSC) (#EDi0001-A) along with the isogenic CRISPr-corrected control line (#EDi0001-A4), in which the start codon of two copies of the SNCA gene were disrupted by CRISPR/Cas (26, 34). Each line was transduced with TetO-Ngn2-Puro as described (60) to establish "NR" (neurogenin-2 + rtTA) iPSCs. Neurogenin-2 mediated differentiation was done as described (60, 61). All iNs were grown on poly-L-ornithine/ laminin pre-coated plates (Biocoat). iNs were used for experiments at between DIV21-24.

Transfections.

Transient transfections were carried out using Lipofectamine 3000 (Invitrogen) according to the manufacturer's instructions.

Acyl-biotin exchange assay (ABE).

Tissue homogenates from frozen brain samples or cells in culture were analyzed by the acyl- biotin exchange assay as described with minor modifications (62). Briefly, mouse whole brain tissue was homogenized using an IKA Microstar 7.5 stirrer set at 750 rpm and a Wheaton/DWK 5 mL tissue grinder (DWK #357974) in 3 mL buffer containing (in mM): 50 Tris, 150 NaCl, 1 EDTA, 1% Triton, 0.1% SDS, 0.1% sodium deoxycholate, supplemented with protease inhibitors. For cells, samples were re-suspended in the same lysis buffer and further extracted with 7 passes through a 27G syringe. For human brain cortical tissue, a small sample of previously frozen tissue was homogenized as above but in buffer containing 50 mM Tris, 1 mM EDTA, and 2% SDS. All extracts were treated with 10 mM NEM for 20 min at 37°C. Proteins were precipitated with acetone and labeled with 0.4 mM pyridyldithiol-biotin (HPDP-biotin) in buffer containing either 0.56 M hydroxylamine or 0.56 M Tris, at pH 7.4, for 1 hour at room temperature. Proteins were run through a Zeba desalting column (Pierce) followed by acetone precipitation. Biotinylated proteins were purified using neutravidin beads (Pierce), eluted with 1% BME, separated by SDS-PAGE, and analyzed by Western blotting.

Immunoblotting.

Cells were lysed in a modified RIPA buffer (50 mM Tris pH 7.4, 1% Triton X-100, 0.1% sodium deoxycholate, 0.1% SDS, 150 mM NaCl, 1 mM EDTA) supplemented with protease and phosphatase inhibitors (Halt, Thermo). Protein concentrations were determined using a Bradford-based assay (Bio-Rad Protein Assay). Equal amounts of protein were loaded and run on NuPAGE 4-12% Bis-Tris gels (Invitrogen). Transfers onto either nitrocellulose or PVDF membranes were performed using template P0 on an iBlot 2 (Invitrogen). For experiments involving detection of αS, membranes were then fixed for 15 min in 4% PFA (in PBS). Blocking was done using 5% milk in PBS. Membranes were incubated in primary antibody in 5% milk in PBST overnight at 4°C. For all experiments involving measurement of $pSer^{129}$ αS, nitrocellulose membranes were used, and blocking was instead done in Odyssey Blocking Buffer, TBS (LI-COR), and primary antibodies diluted in Odyssey Blocking Buffer, TBS supplemented with 0.1% Tween. Imaging of membranes was performed using appropriate secondary antibodies followed by scanning on an Odyssey CLx scanner (LI-COR). For ABE experiments, immunoblotting was done on PVDF membranes and visualized by ECL using SuperSignal West Pico Plus (Thermo) on an iBright CL1500 Western Blot Imaging System (Invitrogen).

Co-immunoprecipitation.

Rat neurons were transduced with either vector control or Syt11-wt-FLAG lentivirus. Between DIV16-19, cells were lysed in 1% Triton, 50 mM Tris, pH 7.4, 150 mM NaCl, 1 mM EDTA supplemented with protease inhibitors and added to 40 μL of washed M2 FLAG affinity gel (Sigma). Proteins were immunoprecipitated overnight with rotation at 4 °C. Affinity gel was washed 3 times in lysis buffer followed by elution in 1x LDS and SDS-PAGE.

Fluorescent imaging and quantification of ZsGreen signal.

Rat neurons were imaged using the Incucyte Zoom (Essen) and ZsGreen fluorescence was quantified using the following processing definition: Adaptive background subtraction, threshold (GCU) 0.1; edge split on, sensitivity 25; cleanup: hole fill 10 μm^2; filters: area (μm^2) min 105, max 500, mean intensity min 28.

Immunofluorescence.

Rat neurons were seeded at $1.5x10^5$ cells per well of a 2-chamber cell imaging cover glass (Eppendorf #0030742010) and transduced with lentivirus if indicated between DIV5-7. Images were acquired on a Leica DMi8 Widefield microscope. Images shown were obtained at 100x. Cells were fixed in 4% paraformaldehyde, permeabilized and blocked in PBS containing 0.1% Triton and 5% goat serum. Samples were incubated overnight at 4 °C with primary antibodies in the same solution, washed with PBS, followed by conjugation to the appropriate Alexa Fluor secondary antibodies. After a second round of washes, cover glasses were mounted to slides with Fluormount G and imaged.

Cycloheximide (CHX) pulse chase experiments.

Cells were treated with 20 μg/mL of CHX (Sigma). At the appropriate time points, cells were lysed and stored for subsequent Western blotting.

Proteasome or lysosome inhibition.

Neurons were treated overnight with either DMSO control, Bafilomycin A (50 nM), epoxomicin (1 μM), or MG132 (5 μM), followed by cell lysis and subsequent Western blotting.

Digitonin-based in situ sequential extraction.

Digitonin-based in situ sequential extraction was performed precisely as described previously (28).

Intact cell cross-linking.

Neurons in 24-well plates were washed in HBSS containing calcium and magnesium to prevent cell detachment. Next, cells were crosslinked in 1 mM final concentration of disuccinimidyl glutarate (DSG) (Thermo Fisher) for 30 min at 37°C without shaking. The reaction was halted by the addition of 50 mM Tris pH 7.5 (final concentration) and incubating at 15 min on the bench at room temperature. Cells were lysed in modified RIPA buffer and prepared for immunoblotting as described above.

Supplementary Material

Refer to Web version on PubMed Central for supplementary material.

Acknowledgements:

We thank the iPSC Neurohub at Brigham and Women's Hospital for generating the *SNCA* triplication and corrected iNs. We thank the NeuroTechnology Studio, also at Brigham and Women's Hospital, for providing instrument access and consultation on data acquisition.

Funding:

This work was supported by NIH grants K08 NS110876 (to G.P.H.) and RF1 NS083845 (to D.J.S.).

Data and materials availability:

All data needed to evaluate the conclusions in the paper are present in the paper or the Supplementary Materials.

References and Notes

1. Consortium IPDG, Imputation of sequence variants for identification of genetic risks for Parkinson's disease: a meta-analysis of genome-wide association studies. Lancet. 377, 641–649 (2011). [PubMed: 21292315]
2. Nalls MA, Pankratz N, Lill CM, Do CB, Hernandez DG, Saad M, DeStefano AL, Kara E, Bras J, Sharma M, Schulte C, Keller MF, Arepalli S, Letson C, Edsall C, Stefansson H, Liu X, Pliner H, Lee JH, Cheng R, I. P. D. G. C. (IPDGC), P. S. G. (PSG) P. R. T. O. Gen. I. (PROGENI), 23andMe, GenePD, N. R. C. (NGRC), H. I. of H. G. (HIHG), A. J. D. Investigator, C. for H. and A. R. in G. E. (CHARGE), N. A. B. E. C. (NABEC), U. K. B. E. C. (UKBEC), G. P. D. Consortium, A. G. A. Group, Ikram MA, Ioannidis JPA, Hadjigeorgiou GM, Bis JC, Martinez M, Perlmutter JS, Goate A, Marder K, Fiske B, Sutherland M, Xiromerisiou G, Myers RH, Clark LN, Stefansson K, Hardy JA, Heutink P, Chen H, Wood NW, Houlden H, Payami H, Brice A, Scott WK, Gasser T, Bertram L, Eriksson N, Foroud T, Singleton AB, Large-scale meta-analysis of genome-wide association data identifies six new risk loci for Parkinson's disease. Nat Genet. 46, 989–993 (2014). [PubMed: 25064009]
3. Sesar A, Cacheiro P, López-López M, Camiña-Tato M, Quintáns B, Monroy-Jaramillo N, Alonso-Vilatela M-E, Cebrián E, Yescas-Gómez P, Ares B, Rivas M-T, Castro A, Carracedo A, Sobrido M-J, Synaptotagmin XI in Parkinson's disease: New evidence from an association study in Spain and Mexico. J Neurol Sci. 362, 321–325 (2016). [PubMed: 26944171]
4. Rudakou U, Yu E, Krohn L, Ruskey JA, Asayesh F, Dauvilliers Y, Spiegelman D, Greenbaum L, Fahn S, Waters CH, Dupré N, Rouleau GA, Hassin-Baer S, Fon EA, Alcalay RN, Gan-Or Z, Targeted sequencing of Parkinson's disease loci genes highlights SYT11, FGF20 and other associations. Brain. 144, 462–472 (2020).
5. Wolfes AC, Dean C, The diversity of synaptotagmin isoforms. Curr Opin Neurobiol. 63, 198–209 (2020). [PubMed: 32663762]
6. Dai H, Shin O-H, Machius M, Tomchick DR, Südhof TC, Rizo J, Structural basis for the evolutionary inactivation of Ca2+ binding to synaptotagmin 4. Nat Struct Mol Biol. 11, 844–849 (2004). [PubMed: 15311271]
7. Fagerberg L, Hallström BM, Oksvold P, Kampf C, Djureinovic D, Odeberg J, Habuka M, Tahmasebpoor S, Danielsson A, Edlund K, Asplund A, Sjöstedt E, Lundberg E, Szigyarto CA-K, Skogs M, Takanen JO, Berling H, Tegel H, Mulder J, Nilsson P, Schwenk JM, Lindskog C, Danielsson F, Mardinoglu A, Sivertsson Å, von Feilitzen K, Forsberg M, Zwahlen M, Olsson I, Navani S, Huss M, Nielsen J, Ponten F, Uhlén M, Analysis of the Human Tissue-specific Expression by Genome-wide Integration of Transcriptomics and Antibody-based Proteomics*. Mol Cell Proteomics. 13, 397–406 (2014). [PubMed: 24309898]
8. Shimojo M, Madara J, Pankow S, Liu X, Yates J, Südhof TC, Maximov A, Synaptotagmin-11 mediates a vesicle trafficking pathway that is essential for development and synaptic plasticity. Genes & development. 33, 365–376 (2019). [PubMed: 30808661]
9. Wang C, Wang Y, Hu M, Chai Z, Wu Q, Huang R, Han W, Zhang CX, Zhou Z, Synaptotagmin-11 inhibits clathrin-mediated and bulk endocytosis. Embo Rep. 17, 47–63 (2016). [PubMed: 26589353]
10. Li W, Wang Y, Li C, Gao P, Zhang F, Hu M, Li J, Zhang S, Li R, Zhang CX, Synaptotagmin-11 inhibits spontaneous neurotransmission through vti1a. J Neurochem. 159, 729–741 (2021). [PubMed: 34599505]

11. Wang C, Kang X, Zhou L, Chai Z, Wu Q, Huang R, Xu H, Hu M, Sun X, Sun S, Li J, Jiao R, Zuo P, Zheng L, Yue Z, Zhou Z, Synaptotagmin-11 is a critical mediator of parkin-linked neurotoxicity and Parkinson's disease-like pathology. Nat Commun. 9, 81 (2018). [PubMed: 29311685]
12. Spillantini MG, Schmidt ML, Lee VM, Trojanowski JQ, Jakes R, Goedert M, Alpha-synuclein in Lewy bodies. Nature. 388, 839–840 (1997). [PubMed: 9278044]
13. Davidson WS, Jonas A, Clayton DF, George JM, Stabilization of α-Synuclein Secondary Structure upon Binding to Synthetic Membranes*. J Biol Chem. 273, 9443–9449 (1998). [PubMed: 9545270]
14. Abeliovich A, Gitler AD, Defects in trafficking bridge Parkinson's disease pathology and genetics. Nature. 539, 207–216 (2016). [PubMed: 27830778]
15. Román-Vendrell C, Medeiros AT, Sanderson JB, Jiang H, Bartels T, Morgan JR, Effects of Excess Brain-Derived Human α-Synuclein on Synaptic Vesicle Trafficking. Front Neurosci-switz. 15, 639414 (2021).
16. Fonseca-Ornelas L, Viennet T, Rovere M, Jiang H, Liu L, Nuber S, Ericsson M, Arthanari H, Selkoe DJ, Altered conformation of α-synuclein drives dysfunction of synaptic vesicles in a synaptosomal model of Parkinson's disease. Cell Reports. 36, 109333 (2021). [PubMed: 34233191]
17. Shahmoradian SH, Lewis AJ, Genoud C, Hench J, Moors TE, Navarro PP, Castaño-Díez D, Schweighauser G, Graff-Meyer A, Goldie KN, Sütterlin R, Huisman E, Ingrassia A, de Gier Y, Rozemuller AJM, Wang J, Paepe AD, Erny J, Staempfli A, Hoernschemeyer J, Großerüschkamp F, Niedieker D, El-Mashtoly SF, Quadri M, IJcken WFJV, Bonifati V, Gerwert K, Bohrmann B, Frank S, Britschgi M, Stahlberg H, de Berg WDJV, Lauer ME, Lewy pathology in Parkinson's disease consists of crowded organelles and lipid membranes. Nat Neurosci. 22, 1099–1109 (2019). [PubMed: 31235907]
18. Kang R, Swayze R, Lise MF, Gerrow K, Mullard A, Honer WG, El-Husseini A, Presynaptic trafficking of synaptotagmin I is regulated by protein palmitoylation. The Journal of biological chemistry. 279, 50524–50536 (2004). [PubMed: 15355980]
19. Flannery AR, Czibener C, Andrews NW, Palmitoylation-dependent association with CD63 targets the Ca2+ sensor synaptotagmin VII to lysosomes. J Cell Biology. 191, 599–613 (2010).
20. Ho GPH, Ramalingam N, Imberdis T, Wilkie EC, Dettmer U, Selkoe DJ, Upregulation of Cellular Palmitoylation Mitigates α-Synuclein Accumulation and Neurotoxicity. Movement Disord. 36, 348–359 (2020). [PubMed: 33103814]
21. Drisdel RC, Alexander JK, Sayeed A, Green WN, Assays of protein palmitoylation. Methods. 40, 127–134 (2006). [PubMed: 17012024]
22. Wan J, Roth AF, Bailey AO, Davis NG, Palmitoylated proteins: purification and identification. Nat Protoc. 2, 1573–1584 (2007). [PubMed: 17585299]
23. Craven SE, El-Husseini AE, Bredt DS, Synaptic Targeting of the Postsynaptic Density Protein PSD-95 Mediated by Lipid and Protein Motifs. Neuron. 22, 497–509 (1999). [PubMed: 10197530]
24. Heindel U, Schmidt MFG, Veit M, Palmitoylation sites and processing of synaptotagmin I, the putative calcium sensor for neurosecretion. Febs Lett. 544, 57–62 (2003). [PubMed: 12782290]
25. Collins MO, Woodley KT, Choudhary JS, Global, site-specific analysis of neuronal protein S-acylation. Sci Rep-uk. 7, 4683 (2017).
26. Devine MJ, Ryten M, Vodicka P, Thomson AJ, Burdon T, Houlden H, Cavaleri F, Nagano M, Drummond NJ, Taanman J-W, Schapira AH, Gwinn K, Hardy J, Lewis PA, Kunath T, Parkinson's disease induced pluripotent stem cells with triplication of the α-synuclein locus. Nat Commun. 2, 440 (2011). [PubMed: 21863007]
27. Tai H-C, Schuman EM, Ubiquitin, the proteasome and protein degradation in neuronal function and dysfunction. Nat Rev Neurosci. 9, 826–838 (2008). [PubMed: 18931696]
28. Ramalingam N, Dettmer U, Temperature is a key determinant of alpha- and beta-synuclein membrane interactions in neurons. J Biol Chem. 296, 100271 (2021). [PubMed: 33428933]
29. Chamberlain LH, Shipston MJ, The Physiology of Protein S-acylation. Physiol Rev. 95, 341–376 (2015). [PubMed: 25834228]

30. Hatzakis NS, Bhatia VK, Larsen J, Madsen KL, Bolinger P-Y, Kunding AH, Castillo J, Gether U, Hedegård P, Stamou D, How curved membranes recruit amphipathic helices and protein anchoring motifs. Nat Chem Biol. 5, 835–841 (2009). [PubMed: 19749743]

31. Larsen JB, Jensen MB, Bhatia VK, Pedersen SL, Bjørnholm T, Iversen L, Uline M, Szleifer I, Jensen KJ, Hatzakis NS, Stamou D, Membrane curvature enables N-Ras lipid anchor sorting to liquid-ordered membrane phases. Nat Chem Biol. 11, 192–194 (2015). [PubMed: 25622090]

32. Medeiros AT, Soll LG, Tessari I, Bubacco L, Morgan JR, α-Synuclein Dimers Impair Vesicle Fission during Clathrin-Mediated Synaptic Vesicle Recycling. Front Cell Neurosci. 11, 388 (2017). [PubMed: 29321725]

33. Perlmutter JD, Braun AR, Sachs JN, Curvature Dynamics of α-Synuclein Familial Parkinson Disease Mutants*. J Biol Chem. 284, 7177–7189 (2009). [PubMed: 19126542]

34. Chen Y, Dolt KS, Kriek M, Baker T, Downey P, Drummond NJ, Canham MA, Natalwala A, Rosser S, Kunath T, Engineering synucleinopathy-resistant human dopaminergic neurons by CRISPR-mediated deletion of the SNCA gene. Eur J Neurosci. 49, 510–524 (2019). [PubMed: 30472757]

35. Dettmer U, Rationally Designed Variants of α-Synuclein Illuminate Its in vivo Structural Properties in Health and Disease. Front Neurosci-switz. 12, 623 (2018).

36. Tripathi A, Alnakhala H, Terry-Kantor E, Newman A, Liu L, Imberdis T, Fanning S, Nuber S, Ramalingam N, Selkoe D, Dettmer U, Pathogenic Mechanisms of Cytosolic and Membrane-Enriched α-Synuclein Converge on Fatty Acid Homeostasis. J Neurosci. 42, 2116–2130 (2022). [PubMed: 35086904]

37. Dettmer U, Newman AJ, Luth ES, Bartels T, Selkoe D, In Vivo Cross-linking Reveals Principally Oligomeric Forms of α-Synuclein and β-Synuclein in Neurons and Non-neural Cells. J Biol Chem. 288, 6371–6385 (2013). [PubMed: 23319586]

38. Dettmer U, Newman AJ, Soldner F, Luth ES, Kim NC, von Saucken VE, Sanderson JB, Jaenisch R, Bartels T, Selkoe D, Parkinson-causing α-synuclein missense mutations shift native tetramers to monomers as a mechanism for disease initiation. Nat Commun. 6, 7314 (2015). [PubMed: 26076669]

39. Kim S, Yun SP, Lee S, Umanah GE, Bandaru VVR, Yin X, Rhee P, Karuppagounder SS, Kwon S-H, Lee H, Mao X, Kim D, Pandey A, Lee G, Dawson VL, Dawson TM, Ko HS, GBA1 deficiency negatively affects physiological α-synuclein tetramers and related multimers. Proc National Acad Sci. 115, 798–803 (2018).

40. Bartels T, Choi JG, Selkoe DJ, α-Synuclein occurs physiologically as a helically folded tetramer that resists aggregation. Nature. 477, 107–110 (2011). [PubMed: 21841800]

41. Wang L, Das U, Scott DA, Tang Y, McLean PJ, Roy S, α-Synuclein Multimers Cluster Synaptic Vesicles and Attenuate Recycling. Curr Biol. 24, 2319–2326 (2014). [PubMed: 25264250]

42. Muntané G, Ferrer I, Martinez-Vicente M, α-synuclein phosphorylation and truncation are normal events in the adult human brain. Neuroscience. 200, 106–119 (2012). [PubMed: 22079575]

43. McFarland NR, Fan Z, Xu K, Schwarzschild MA, Feany MB, Hyman BT, McLean PJ, α-Synuclein S129 Phosphorylation Mutants Do Not Alter Nigrostriatal Toxicity in a Rat Model of Parkinson Disease. J Neuropathology Exp Neurology. 68, 515–524 (2009).

44. Oueslati A, Schneider BL, Aebischer P, Lashuel HA, Polo-like kinase 2 regulates selective autophagic α-synuclein clearance and suppresses its toxicity in vivo. Proc National Acad Sci. 110, E3945–E3954 (2013).

45. Fujiwara H, Hasegawa M, Dohmae N, Kawashima A, Masliah E, Goldberg MS, Shen J, Takio K, Iwatsubo T, alpha-Synuclein is phosphorylated in synucleinopathy lesions. Nature cell biology. 4, 160–164 (2002). [PubMed: 11813001]

46. Ma M-R, Hu Z-W, Zhao Y-F, Chen Y-X, Li Y-M, Phosphorylation induces distinct alpha-synuclein strain formation. Sci Rep-uk. 6, 37130 (2016).

47. Zarranz JJ, Alegre J, Gómez-Esteban JC, Lezcano E, Ros R, Ampuero I, Vidal L, Hoenicka J, Rodriguez O, Atarés B, Llorens V, Tortosa EG, del Ser T, Muñoz DG, de Yebenes JG, The new mutation, E46K, of α-synuclein causes parkinson and Lewy body dementia. Ann Neurol. 55, 164–173 (2004). [PubMed: 14755719]

48. Mbefo MK, Fares M-B, Paleologou K, Oueslati A, Yin G, Tenreiro S, Pinto M, Outeiro T, Zweckstetter M, Masliah E, Lashuel HA, Parkinson Disease Mutant E46K Enhances α-Synuclein Phosphorylation in Mammalian Cell Lines, in Yeast, and in Vivo *. J Biol Chem. 290, 9412–9427 (2015). [PubMed: 25657004]
49. Cooper AA, Gitler AD, Cashikar A, Haynes CM, Hill KJ, Bhullar B, Liu K, Xu K, Strathearn KE, Liu F, Cao S, Caldwell KA, Caldwell GA, Marsischky G, Kolodner RD, LaBaer J, Rochet J-C, Bonini NM, Lindquist S, α-Synuclein Blocks ER-Golgi Traffic and Rab1 Rescues Neuron Loss in Parkinson9s Models. Science. 313, 324–328 (2006). [PubMed: 16794039]
50. Huynh DP, Scoles DR, Nguyen D, Pulst SM, The autosomal recessive juvenile Parkinson disease gene product, parkin, interacts with and ubiquitinates synaptotagmin XI. Human molecular genetics. 12, 2587–2597 (2003). [PubMed: 12925569]
51. Narendra D, Walker JE, Youle R, Mitochondrial Quality Control Mediated by PINK1 and Parkin: Links to Parkinsonism. Csh Perspect Biol. 4, a011338 (2012).
52. Ordureau A, Paulo JA, Zhang W, Ahfeldt T, Zhang J, Cohn EF, Hou Z, Heo J-M, Rubin LL, Sidhu SS, Gygi SP, Harper JW, Dynamics of PARKIN-Dependent Mitochondrial Ubiquitylation in Induced Neurons and Model Systems Revealed by Digital Snapshot Proteomics. Mol Cell. 70, 211–227.e8 (2018). [PubMed: 29656925]
53. Ordureau A, Paulo JA, Zhang J, An H, Swatek KN, Cannon JR, Wan Q, Komander D, Harper JW, Global Landscape and Dynamics of Parkin and USP30-Dependent Ubiquitylomes in iNeurons during Mitophagic Signaling. Mol Cell. 77, 1124–1142.e10 (2020). [PubMed: 32142685]
54. Antico O, Ordureau A, Stevens M, Singh F, Nirujogi RS, Gierlinski M, Barini E, Rickwood ML, Prescott A, Toth R, Ganley IG, Harper JW, Muqit MMK, Global ubiquitylation analysis of mitochondria in primary neurons identifies endogenous Parkin targets following activation of PINK1. Sci Adv. 7, eabj0722 (2021). [PubMed: 34767452]
55. Anderson JP, Walker DE, Goldstein JM, de Laat R, Banducci K, Caccavello RJ, Barbour R, Huang J, Kling K, Lee M, Diep L, Keim PS, Shen X, Chataway T, Schlossmacher MG, Seubert P, Schenk D, Sinha S, Gai WP, Chilcote TJ, Phosphorylation of Ser-129 Is the Dominant Pathological Modification of α-Synuclein in Familial and Sporadic Lewy Body Disease*. J Biol Chem. 281, 29739–29752 (2006). [PubMed: 16847063]
56. Nuber S, Rajsombath M, Minakaki G, Winkler J, Müller CP, Ericsson M, Caldarone B, Dettmer U, Selkoe DJ, Abrogating Native α-Synuclein Tetramers in Mice Causes a L-DOPA-Responsive Motor Syndrome Closely Resembling Parkinson's Disease. Neuron. 100, 75–90.e5 (2018). [PubMed: 30308173]
57. Imberdis T, Negri J, Ramalingam N, Terry-Kantor E, Ho GPH, Fanning S, Stirtz G, Kim T-E, Levy OA, Young-Pearse TL, Selkoe D, Dettmer U, Cell models of lipid-rich α-synuclein aggregation validate known modifiers of α-synuclein biology and identify stearoyl-CoA desaturase. Proc National Acad Sci. 116, 20760–20769 (2019).
58. Fanning S, Cirka H, Thies JL, Jeong J, Niemi SM, Yoon J, Ho GPH, Pacheco JA, Dettmer U, Liu L, Clish CB, Hodgetts KJ, Hutchinson JN, Muratore CR, Caldwell GA, Caldwell KA, Selkoe D, Lipase regulation of cellular fatty acid homeostasis as a Parkinson's disease therapeutic strategy. Npj Park Dis. 8, 74 (2022).
59. Mazzulli JR, Zunke F, Isacson O, Studer L, Krainc D, α-Synuclein–induced lysosomal dysfunction occurs through disruptions in protein trafficking in human midbrain synucleinopathy models. Proc National Acad Sci. 113, 1931–1936 (2016).
60. Nehme R, Zuccaro E, Ghosh SD, Li C, Sherwood JL, Pietilainen O, Barrett LE, Limone F, Worringer KA, Kommineni S, Zang Y, Cacchiarelli D, Meissner A, Adolfsson R, Haggarty S, Madison J, Muller M, Arlotta P, Fu Z, Feng G, Eggan K, Combining NGN2 Programming with Developmental Patterning Generates Human Excitatory Neurons with NMDAR-Mediated Synaptic Transmission. Cell Reports. 23, 2509–2523 (2018). [PubMed: 29791859]
61. Zhang Y, Pak C, Han Y, Ahlenius H, Zhang Z, Chanda S, Marro S, Patzke C, Acuna C, Covy J, Xu W, Yang N, Danko T, Chen L, Wernig M, Südhof TC, Rapid single-step induction of functional neurons from human pluripotent stem cells. Neuron. 78, 785–798 (2013). [PubMed: 23764284]
62. Ho GPH, Selvakumar B, Mukai J, Hester LD, Wang Y, Gogos JA, Snyder SH, S-Nitrosylation and S-Palmitoylation Reciprocally Regulate Synaptic Targeting of PSD-95. Neuron. 71, 131–141 (2011). [PubMed: 21745643]

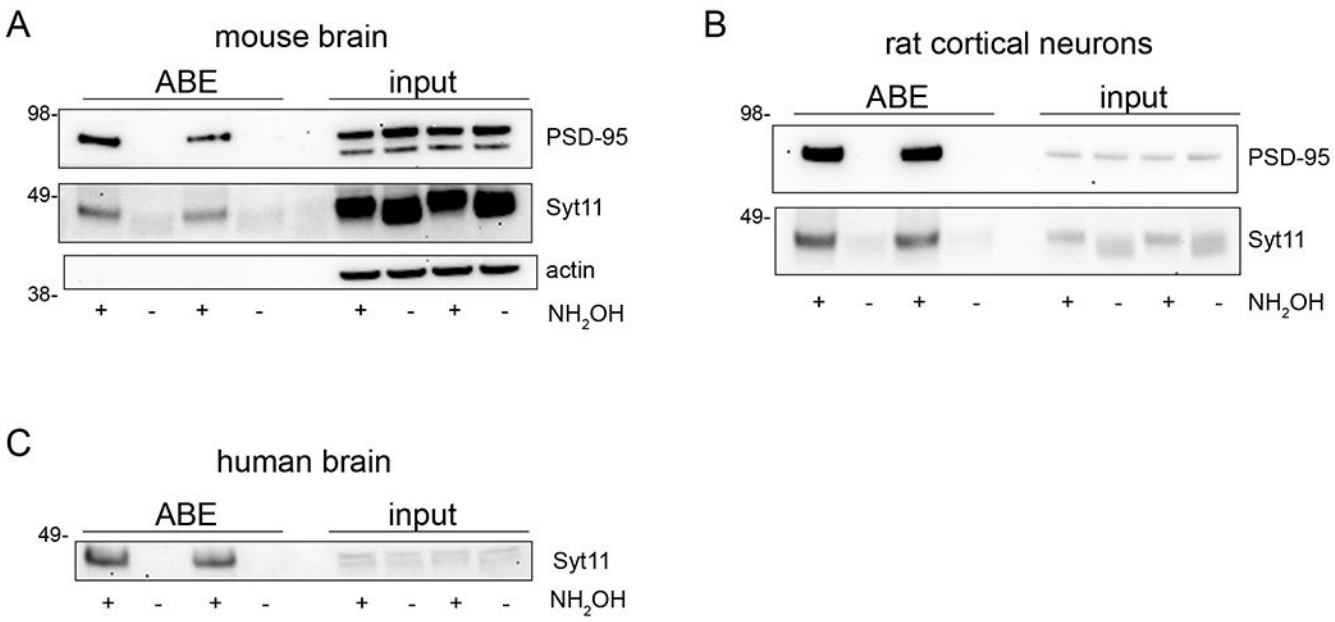

Figure 1. Syt11 is physiologically palmitoylated.

(A) Palmitoylation of Syt11 in mouse brain (homogenized tissue in modified RIPA buffer), analyzed by the ABE assay. Hydroxylamine (NH_2OH) dependence was a control for signal specificity; PSD-95 and actin are positive and negative control proteins, respectively, for the ABE assay. 5% of the total lysate was used for input. **(B)** Palmitoylation of Syt11 and PSD-95 in rat cortical neuronal cultures, analyzed as in (A). **(C)** Palmitoylation of Syt11 in human brain tissue, extracted in 2% SDS, otherwise analyzed as in (A). Blots in (A to C) are representative of 3 independent samples.

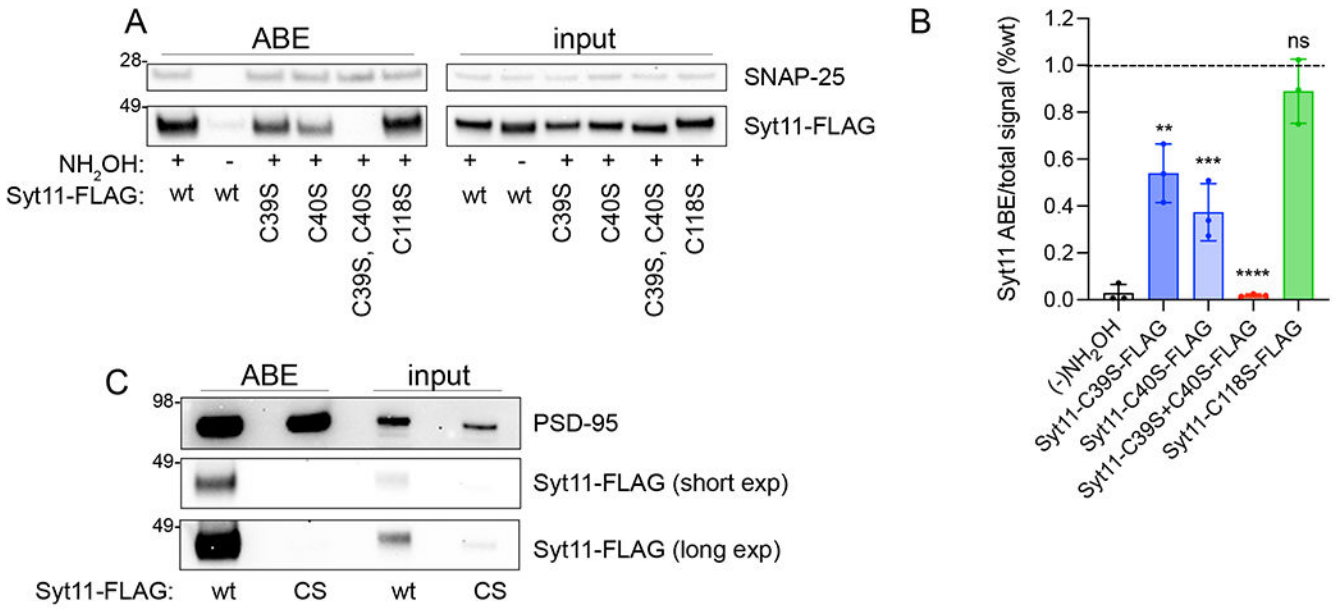

Figure 2. Syt11 is palmitoylated at Cys^{39} and Cys^{40}.

(A) HEK293 cells were transfected with the indicated FLAG-tagged mutant constructs of Syt11 and analyzed for palmitoylation by ABE assay. **(B)** Quantification of (A). Data are plotted as mean ±SD from n = 3 biological replicates, analyzed by one-way ANOVA with Sidak's multiple comparisons: ** P<0.01, *** P<0.001, and **** P<0.0001; ns, not significant. **(C)** Rat cortical neurons were transduced with lentivirus encoding Syt11-wt-FLAG or Syt11-C39S/C40S-FLAG (abbreviated "CS") and analyzed by ABE.

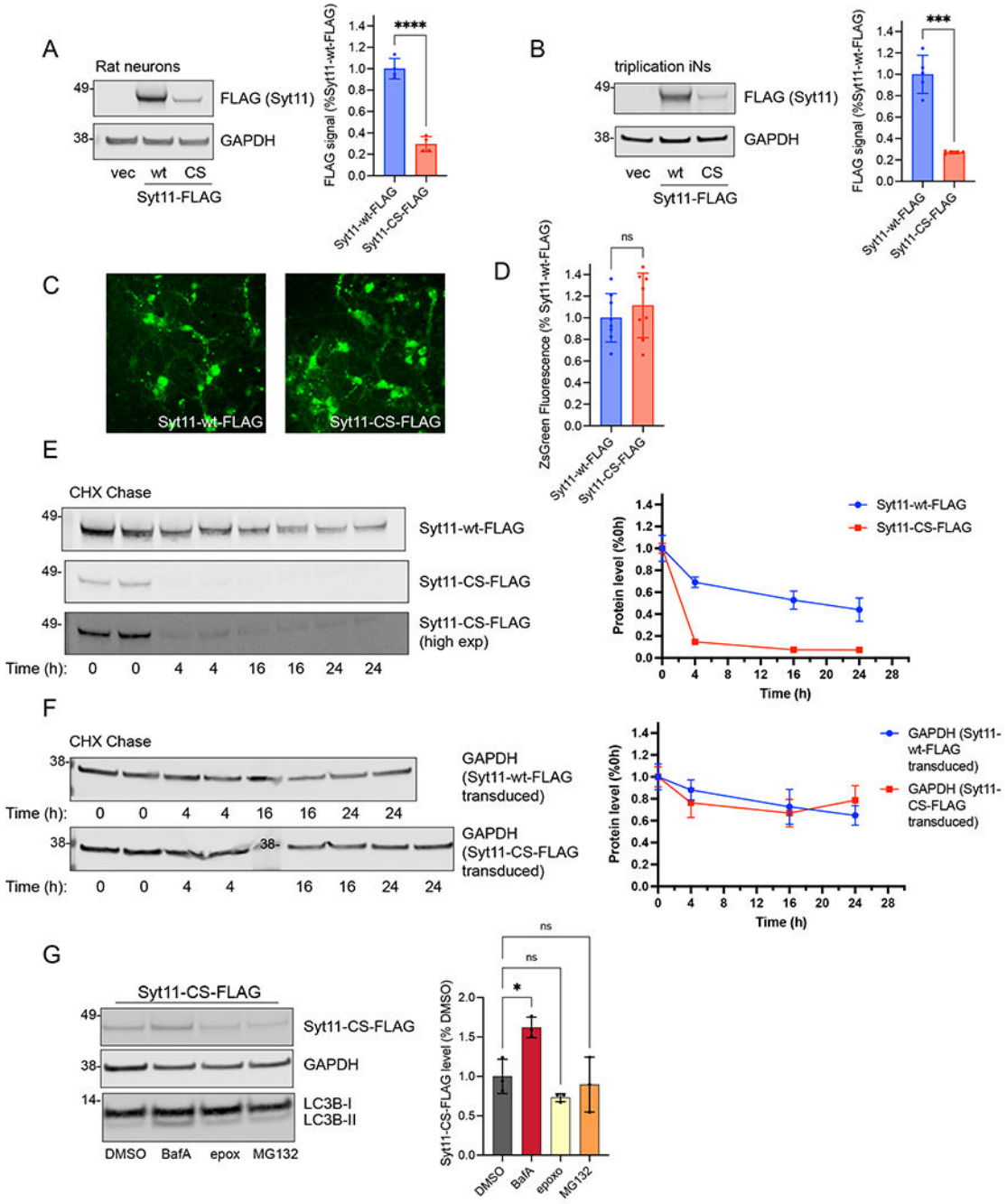

Figure 3. Palmitoylation of Syt11 regulates its degradation by the endosomal-lysosomal system.

(A) Rat cortical neurons were transduced with lentivirus containing a bicistronic vector encoding either Syt11-wt-FLAG or the palmitoylation-deficient (CS) mutant together with a ZsGreen1 reporter. Protein levels were analyzed by Western blot and quantified (right). Data are plotted as means ±SD from n = 4 biological replicates, analyzed by unpaired t-test: ****P<0.0001. **(B)** Human *SNCA* gene triplication induced neurons (iNs) were transduced, and protein levels were measured, as in (A) with quantification (right). Data are plotted as means ±SD from n = 5 biological replicates, analyzed by unpaired t-test: ***P<0.001.

(C) Representative images of rat neurons from (A) transduced with either Syt11-wt-FLAG or Syt11-CS-FLAG. **(D)** Quantification of the ZsGreen1 signal in (C), expressed as % of the Syt11-wt-FLAG condition. Data are plotted as means ±SD from n = 8 fields from 4 biological replicates, analyzed by unpaired t-test: ns, not significant. **(E)** Rat neurons transduced with either Syt11-wt-FLAG or Syt11-CS-FLAG were treated with cycloheximide (CHX) for the indicated times and protein levels analyzed by WB, expressed as % that at 0 hours. Data are plotted as means ±SD from n = 3 biological replicates. **(F)** GAPDH protein levels from experiments in (E) were examined. Data are plotted as means ±SD from n = 3 biological replicates. **(G)** Rat neurons expressing Syt11-CS-FLAG were treated with the lysosomal inhibitor bafilomycin A (BafA, 50 nM) or proteasomal inhibitor epoxomycin (epox, 1 μM) or MG132 (5 μM), as indicated, followed by analysis of Syt11 protein levels. LC3B levels are used as a marker of lysosomal inhibition. Data are plotted as means ±SD from n = 3 biological replicates, analyzed by one-way ANOVA with Dunnett's multiple comparisons. *P<0.05; ns, not significant.

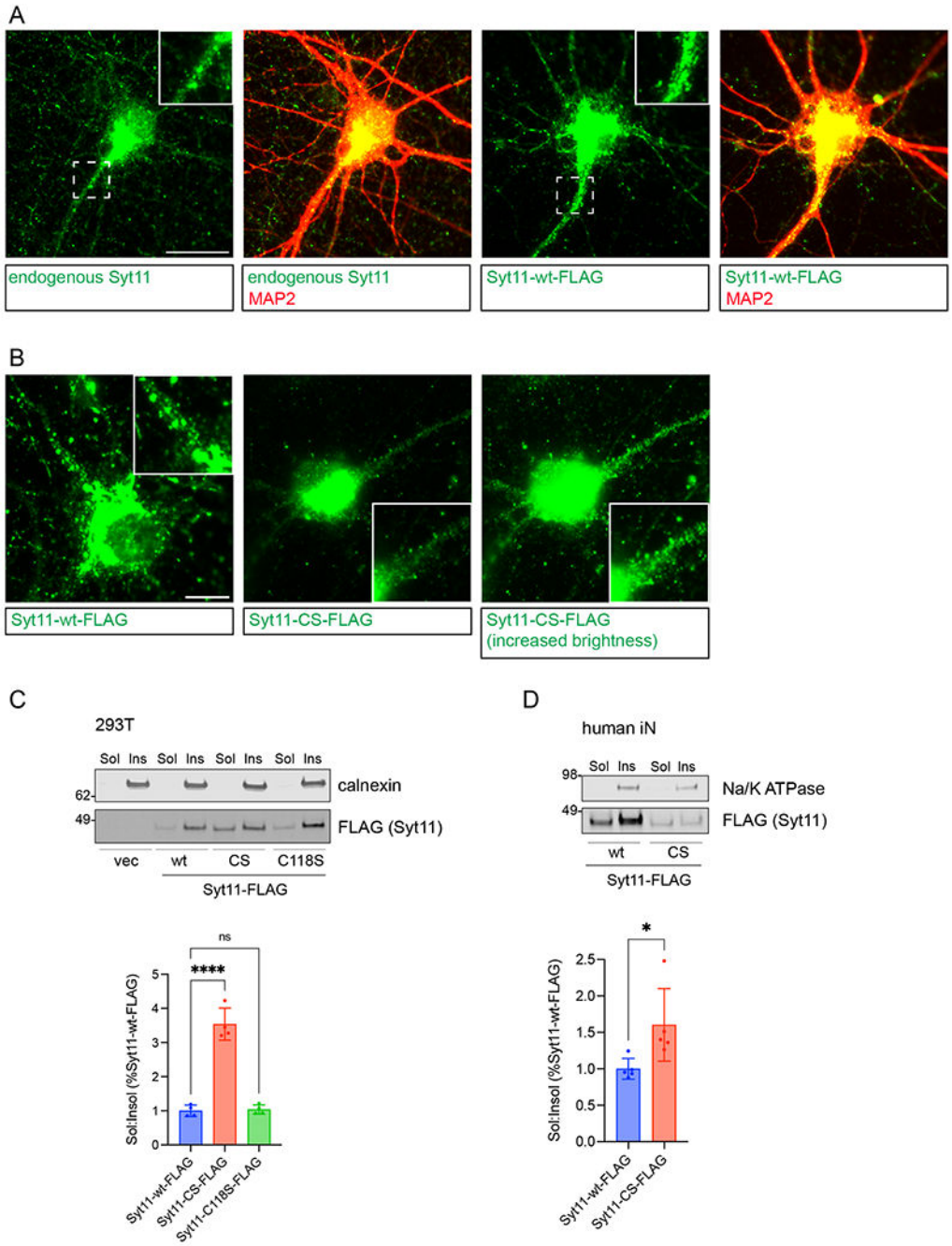

Figure 4. Palmitoylation of Syt11 confers resistance to digitonin extraction from membranes without broadly affecting Syt11 localization.

(A) Rat neurons were transduced with Syt11-wt-FLAG lentivirus or left untreated followed by immunofluorescence imaging for endogenous Syt11 and MAP2. Scale bar, 20 μm. **(B)** Rat neurons were transduced with Syt11-wt-FLAG lentivirus (MOI 5) or Syt11-CS-FLAG lentivirus (MOI 20), immunostained with FLAG antibodies, and imaged. Right-most panel contains an artificially brightened version of the image in the middle panel. Scale bar, 10 μm. **(C)** 293T cells were transfected with the indicated wild-type or mutant construct of

Syt11 and subjected to 800 μg/mL digitonin extraction. The digitonin-extractable fraction is designated “Sol” (for digitonin soluble), and the resistant fraction is designated “Ins” (or “Insol” in the graphs; for digitonin insoluble). Membrane marker calnexin was a control for consistency of extractions for each mutant. Data are plotted as means ±SD from n = 4 biological replicates, analyzed by one-way ANOVA with Dunnett’s multiple comparisons: ****$P<0.0001$; ns, not significant. **(D)** Human *SNCA* triplication iNs were transduced with Syt11-wt-FLAG or Syt11-CS-FLAG and subjected to 1000 μg/mL digitonin extraction, and analyzed as in (C), with Na/K ATPase as the control for consistency of the extractions. Data are plotted as means ±SD from n = 5 biological replicates, unpaired t-test: *$P<0.05$.

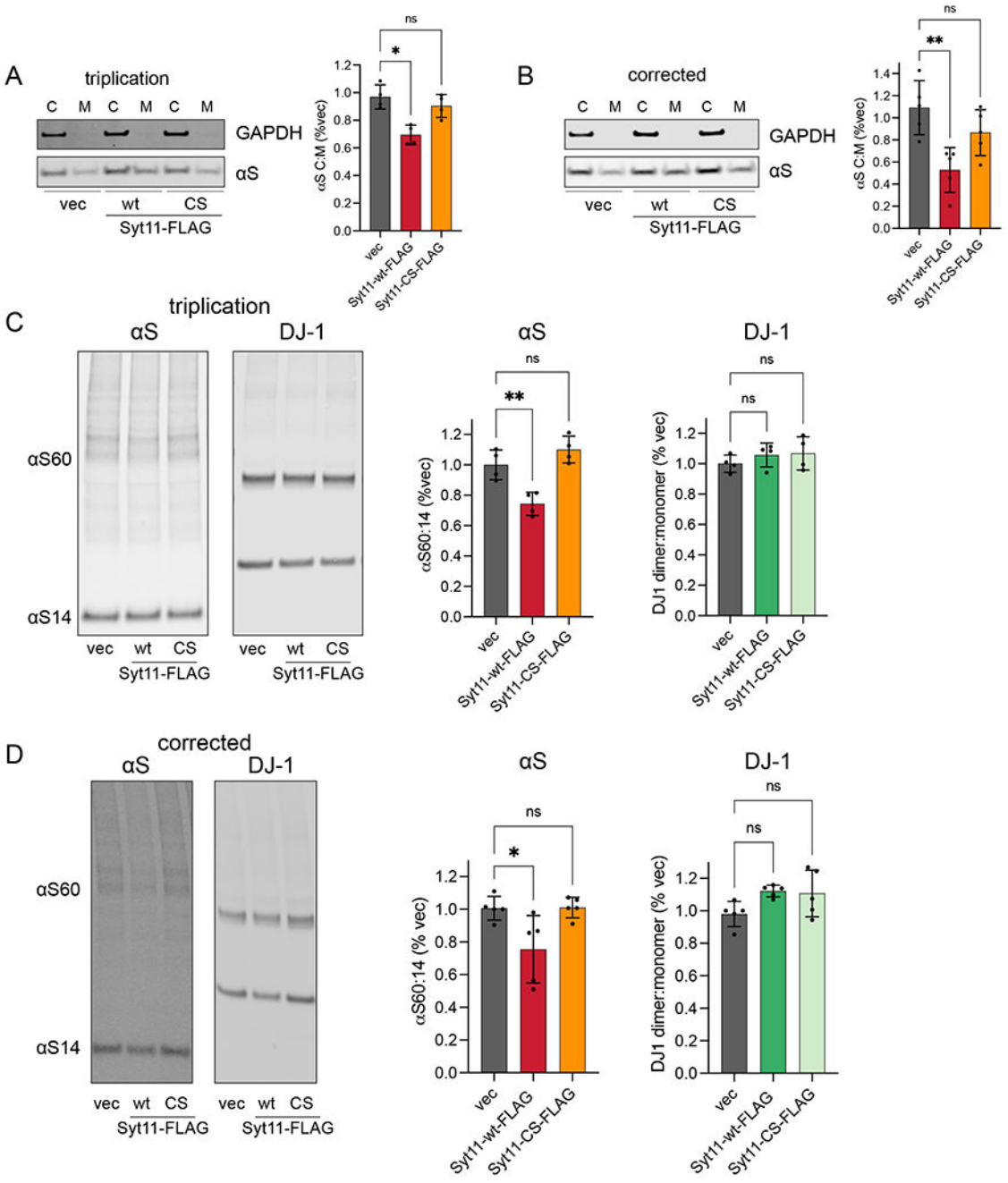

Figure 5. Syt11 modulates αS homeostasis in PD patient-derived neurons.

(A) *SNCA* triplication iNs expressing either Syt11-wt-FLAG or Syt11-CS-FLAG were analyzed by digitonin extraction with 1000 μg/mL of digitonin with quantification (right), calculated as the cytosol (C) to membrane (M) ratio, expressed as a percentage of vector control. Data are plotted as means ±SD from n = 4 biological replicates, analyzed by one-way ANOVA with Dunnett's multiple comparisons: **P*<0.05; ns, not significant. **(B)** *SNCA* triplication-corrected iNs were analyzed as in (A). Data are plotted as means ±SD from n = 5 biological replicates, analyzed by one-way ANOVA with Dunnett's multiple

comparisons: $^{**}P<0.01$; ns, not significant. **(C)** Triplication iNs were transduced as in (A) and αS tetramers measured by intact cell DSG cross-linking. DJ1 was a control for consistency of the cross-linking method across conditions. Data are plotted as means ±SD from n = 4 biological replicates, analyzed by one-way ANOVA with Dunnett's multiple comparisons: $^{**}P<0.01$; ns, not significant. **(D)** Triplication-corrected iNs were analyzed as in (C). Data are plotted as means ±SD from n = 5 biological replicates, analyzed by one-way ANOVA with Dunnett's multiple comparisons: $^{*}P<0.05$; ns, not significant.

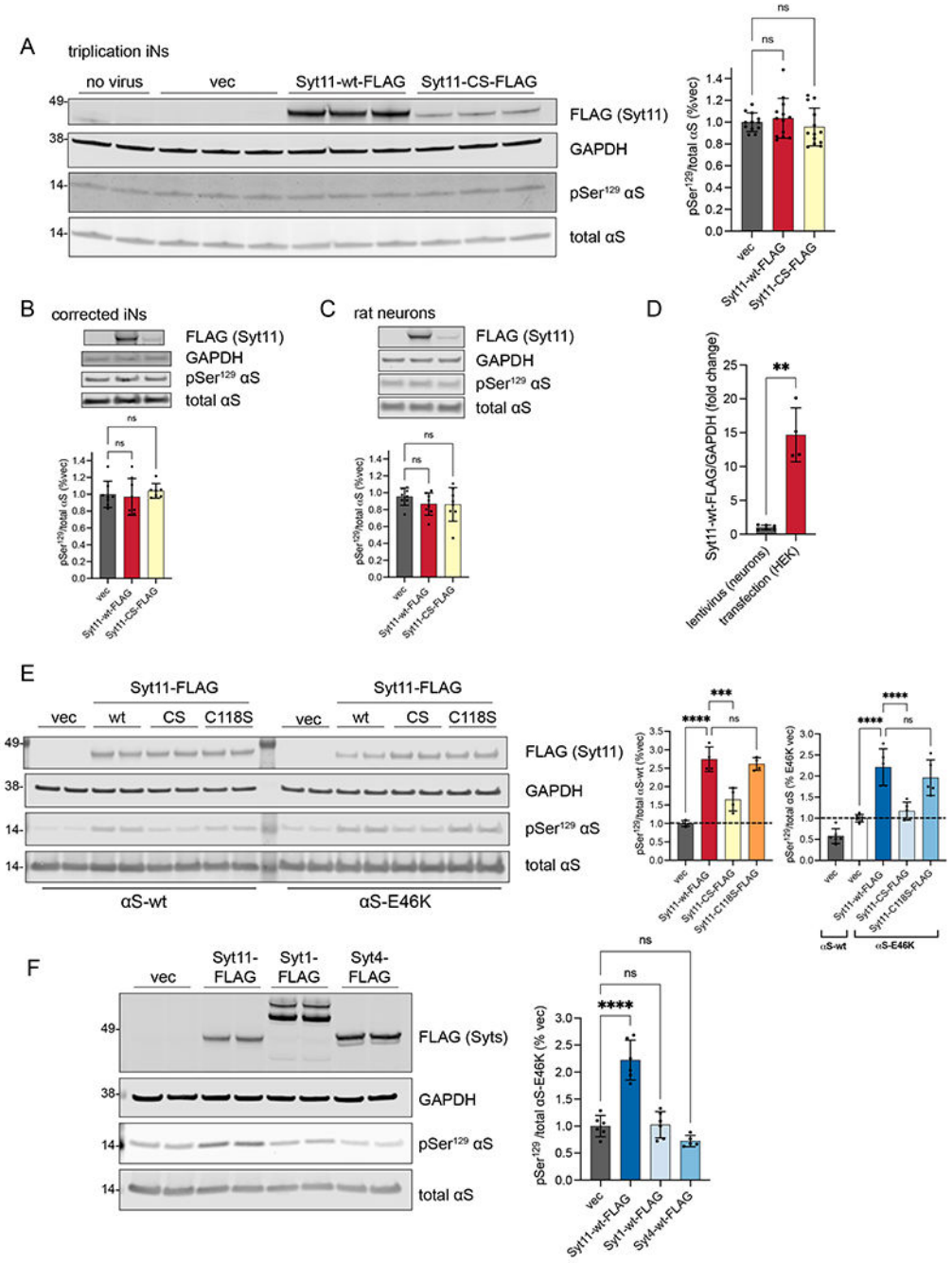

Figure 6. Effect of Syt11 on pSer^{129} αS.

(A) *SNCA* triplication iNs were transduced with the indicated lentiviruses and pSer^{129} αS assessed by WB, normalized to total αS, and quantified as % vector control. Data are plotted as means ±SD from n = 13 biological replicates, analyzed by one-way ANOVA with Dunnett's multiple comparisons: ns, not significant. **(B and C)** *SNCA* triplication-corrected iNs (B) and primary rat neurons (C) were transduced with the indicated lentiviruses followed by assessment of pSer^{129} αS as in (A). Data are plotted as means ±SD from n = 8 biological replicates each, analyzed by one-way ANOVA with Dunnett's multiple comparisons: ns, not

significant. **(D)** Comparison of Syt11-wt-FLAG levels in *SNCA* triplication iNs transduced with Syt11-wt-FLAG and HEK cells transiently transfected with Syt11-wt-FLAG. To ensure valid comparisons across experiments, levels of Syt11-wt-FLAG on WB were normalized to GAPDH levels for each respective condition and expressed as a fold change of Syt11-wt-FLAG levels in the lentivirus transduced iNs. Data are plotted as means ±SD from n=6 biological replicates for iNs and 4 biological replicates for HEK cells, analyzed by unpaired t-test with Welch's correction: $^{**}P<0.01$. **(E)** HEK293 cells were co-transfected with either αS-wt or αS-E46K along with the indicated Syt11 mutants. pSer^{129} αS was measured as in (A). Data are plotted as means ±SD from n = 4 biological replicates for αS-wt and n = 5 biological replicates for αS-E46K, analyzed by one-way ANOVA with Dunnett's multiple comparisons: $^{***}P<0.001$, $^{****}P<0.0001$; ns, not significant. **(F)** HEK293 cells were co-transfected with αS-E46K and either Syt11-wt-FLAG, Syt1-wt-FLAG, or Syt4-wt-FLAG. pSer^{129} was measured, presented, and analyzed as in (A) from n = 6 biological replicates. Statistical analysis: one-way ANOVA with Dunnett's multiple comparisons: $^{****}P<0.0001$; ns, not significant.